ISSN 1063-780X, Plasma Physics Reports, 2013, Vol. 39, No. 4, pp. 296–306. © Pleiades Publishing, Ltd., 2013.
Original Russian Text © S.A. Kurkin, A.A. Koronovskii, A.E. Hramov, 2013, published in Fizika Plazmy, 2013, Vol. 39, No. 4, pp. 333–344.

PLASMA DYNAMICS

Specific Features of Virtual Cathode Formation and Dynamics with Allowance for the Magnetic Self-Field of a Relativistic Electron Beam

S. A. Kurkin*, A. A. Koronovskii, and A. E. Hramov

Saratov State University, Bol'shaya Kazach'ya ul. 112, Saratov, 410012 Russia
Saratov State Technical University, Politekhnicheskaya ul. 77, Saratov, 410054 Russia
**e-mail: kurkinsa@gmail.com*

Received March 27, 2012; in final form, June 27, 2012

Abstract—The conditions and mechanisms of virtual cathode formation in relativistic and ultrarelativistic electron beams are analyzed with allowance for the magnetic self-field for different magnitudes of the external magnetic field. The typical behavior of the critical current at which an oscillating virtual cathode forms in a relativistic electron beam is investigated as a function of the electron energy and the magnitude of the uniform external magnetic field. It is shown that the conditions for virtual cathode formation in a low external magnetic field are determined by the influence of the magnetic self-field of the relativistic electron beam. In particular, azimuthal instability of the electron beam caused by the action of the beam magnetic self-field, which leads to a reduction in the critical current of the relativistic electron beam, is revealed.

DOI: 10.1134/S1063780X13040065

1. INTRODUCTION

The formation of a virtual cathode (VC) in an intense electron beam with a supercritical current is related to the appearance of a potential barrier in the beam drift space, which reflects a fraction of the beam electrons back to the injection plane and to the side surface of the drift space [1–3]. The appearance of such a potential barrier is caused by the space charge of the electron beam injected into the chamber. At low beam currents, the depth of the potential well is small and the entire electron beam passes without reflection to the output plane of the drift space (the regime of stationary beam transport). As the beam current increases (the energy of the beam electrons being fixed), the space charge density in the beam and, accordingly, the depth of the potential well also increase. At a certain beam current, called the limiting (or critical) vacuum current [4, 5], the depth of the potential well becomes sufficient to reflect the beam electrons, which leads to the formation of a VC [1]. It is well known that the VC formed in the electron beam is always unsteady and oscillates in both time and space [2, 6–12]. This enables one to use electron beams with supercritical currents in the VC formation mode for generation of high-power microwave radiation [13–19]. The critical current at which a VC forms in a relativistic electron beam (REB) is the start current for vircators. It is a relatively easily measured characteristic, important for understanding the physical processes occurring in systems with a VC.

The formation and dynamics of the VC were thoroughly studied [9, 10, 14, 20–23] mainly for the case of one-dimensional (1D) motion of the beam electrons (the model of a fully magnetized beam). In the framework of this model, Bogdankevich and Rukhadze [4, 24, 25] derived the following analytic formula for the critical current in the case of a cylindrical interaction space:

$$I_{\mathrm{SCL}} = \frac{c^3}{\eta}\frac{\left(\gamma_0^{2/3}-1\right)^{3/2}}{d/R_b + 2\ln(R/R_b)}, \quad \gamma_0 = \frac{1}{\sqrt{\left(1-v_0^2/c^2\right)}}, \quad (1)$$

where R is the radius of the interaction space; R_b and d are the radius and wall thickness of the annular electron beam, respectively; γ_0 and v_0 are the relativistic factor and velocity of the REB electrons in the injection plane, respectively; c is the speed of light; and η is the electron charge-to-mass ratio. It was shown in [26, 27] that formula (1) for the critical current of a magnetized electron beam agrees well with the experiment.

In recent years, studies of the dynamics of an electron beam with a VC in two-dimensional (2D) and three-dimensional (3D) geometries have attracted considerable interest [18, 28–34]. This is explained by the fact that the 1D theory of a vircator does not take into account some important aspects of the behavior of an electron beam with a VC and, in some cases, disagrees with the experiment. From the practical standpoint, such studies are important for analyzing the characteristics of electromagnetic pulses generated in vircators without an external magnetic field [2, 13, 35] or with a nonuniform magnetic field in the region of VC formation [36–38].

An important line of these studies is analysis of the influence of the external magnetic field on the critical current required for VC formation in an electron beam [1, 39]. Such studies for nonrelativistic and weakly relativistic beams were performed in [31, 40–43] in the framework of quasi-static modeling [32, 40]. It was found that a finite external magnetic field and the effects of 2D electron beam dynamics in such a field significantly affect the mechanisms and conditions of VC formation (including the value of the critical current). This is caused by the fact that, first, the space charge density near the VC depends strongly on the magnitude of the external magnetic field focusing the electron beam and, second, the external magnetic field significantly affects the dynamics of charged particles in the self-consistent field of the space charge. In particular, it was shown in [41–43] that the critical current increases with decreasing external magnetic field due to a reduction in the space charge density in the beam caused by the Coulomb repulsion of electrons, which leads to an increase in the cross section of the electron beam.

At present, the question of the conditions for VC formation in an REB in a finite external magnetic field still remains open. As the REB current and energy increase, a number of effects that are inessential for weakly relativistic beams come into play. In particular, in the case of an REB, it is impossible to disregard the magnetic self-field of the beam, which begins to substantially affect the process of VC formation. Taking into account the magnetic self-field necessitates the use of essentially 3D self-consistent electromagnetic models of the dynamics of an REB with a supercritical current, due to which such studies become very complicated and require large computation resources. Nevertheless, it is absolutely necessary to take into account the magnetic self-field in analyzing modern VC devices, such as relativistic vircators [39] and ion acceleration systems [44, 45]. Therefore, systematic studies of the conditions and mechanisms for VC formation in an REB with allowance for 3D dynamics of the electron beam with a VC is undoubtedly very challenging.

In this work, we present results of 3D numerical electromagnetic simulations of the VC dynamics in an annular REB for different magnitudes of the external uniform magnetic field. Typical behavior of the critical current for VC formation in an REB is investigated as a function of the electron energy and the magnitude of the external uniform magnetic field, and some analytic estimates of the vircator dynamics are presented.

2. MODEL

Let us consider a segment of a cylindrical waveguide of length L and radius R, closed on both ends by grids. An axisymmetric monoenergetic annular REB of radius R_b and wall thickness d with a particle energy W_e and current I is injected into the interaction space through the left (input) grid and is output through the right (output) grid. The beam electrons can also escape to the side wall of the interaction space. In the simulations performed in this work, it was assumed that $L = 40$ mm, $R = 10$ mm, $R_b = 5$ mm, and $d = 2$ mm.

Along the axis of the interaction space, an external uniform focusing magnetic field $B_z = B_0$ is applied. It is assumed that the source of the REB is not screened from the external magnetic field. In this case, the magnetic field at the input to the drift space coincides with that in the region of the beam source, due to which the REB does not acquire an additional azimuthal velocity defined by the Busch theorem [46]. Such a magnetic field distribution is typical of many high-power electronic devices; in particular, of magnetically insulated diodes forming high-current REBs in which the external magnetic field at the cathode coincides with the focusing magnetic field in the drift space [46–48].

In this work, the REB dynamics in the interaction space is described in terms of a nonstationary 3D fully electromagnetic model based on self-consistently solving a set of Maxwell's equations for the electromagnetic field and equations of motion of large model particles simulating the beam electrons [49–51]. It should be noted that, at present, such models are commonly used to analyze physical processes in various high-power vacuum and plasma electronic devices [52]. The equations used in the model have the form

$$\nabla \times \mathbf{E} = -\frac{1}{c}\frac{\partial \mathbf{H}}{\partial t}, \quad \nabla \times \mathbf{H} = \frac{1}{c}\frac{\partial \mathbf{E}}{\partial t} + \frac{4\pi}{c}\mathbf{j}, \tag{2}$$

$$\nabla \cdot \mathbf{E} = 4\pi\rho, \quad \nabla \cdot \mathbf{H} = 0, \tag{3}$$

$$\frac{d\mathbf{p}_i}{dt} = \mathbf{E}_i + (\mathbf{p}_i \times \mathbf{B}_i)/\gamma_i, \quad \frac{d\mathbf{r}_i}{t} = \mathbf{p}_i/\gamma_i, \quad i = 1 \dots N, \tag{4}$$

with the corresponding initial and boundary conditions. Here, $\mathbf{E}$ and $\mathbf{H}$ are the electric and magnetic fields, respectively; ρ and $\mathbf{j}$ are the charge and current densities in the beam, respectively; $\vec{r}$, $\vec{p}$, and γ are the radius vector, momentum, and relativistic factor of a model particle, respectively; the index i refers to the ith model particle; and N is the number of model particles used in the numerical experiment.

The numerical scheme is based on the 3D modification of the 2.5-dimensional scheme developed earlier by us in [18] and consists in the integration of set of equations (2)–(4) with the boundary conditions corresponding to the perfectly conducting wall of the interaction space. Maxwell's equations in cylindrical coordinates are solved in a standard way on mutually

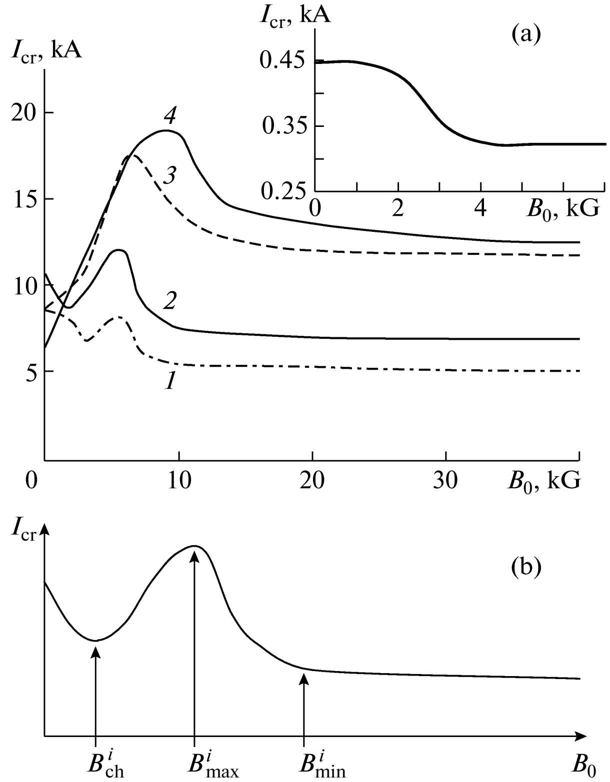

Fig. 1. (a) Critical current of an annular REB vs. external magnetic field for the initial electron energies W_e = (*1*) 0.48, (*2*) 0.6, (*3*), 0.850, and (*4*) 1.0 MeV. The inset (taken from [43]) shows the critical current for a weakly relativistic beam with an electron energy of $W_e = 0.079$ MeV. (b) Schematic plot of the dependence $I_{cr}(B_0)$, on which the characteristic values of the external magnetic field are shown: the value B^i_{ch}, at which the critical current reaches its the first minimal value; B^i_{max}, at which the critical current reaches its local maximum; and B^i_{min}, at which the dependence $I_{cr}(B_0)$ saturates.

shifted space–time grids with a constant time step Δt and constant steps Δz, Δr, and $\Delta\theta$ over the longitudinal, radial, and angular coordinates, respectively, on each of which one of the field components is determined (see [49, 50, 52, 53] for details). The output of the electromagnetic power is modeled using an approach based on the filling of a segment of the electrodynamic system (waveguide) $L > z > 1.2L$ with a conducting medium with the conductivity σ [50, 54].

The relativistic equations of motion of model particles (see Eqs. (4)) are solved using the Boris algorithm in cylindrical coordinates [55]. In this case, three components of the velocity $\mathbf{v}$ of a charged particle (the longitudinal component v_z, radial component v_r, and azimuthal component v_θ) are calculated. The space charge density $\rho(\mathbf{r}, t)$ and current density $\mathbf{j}(\mathbf{r}, t)$ of the REB are found using the standard procedure of linear weighting on a grid (the cloud-in-cell (CIC) method) in three cylindrical coordinates [50].

3. CONDITIONS AND MECHANISMS OF VC FORMATION IN AN ANNULAR REB

3.1. Conditions of VC Formation and REB Critical Current for Different Magnitudes of the External Magnetic Field

Let us consider the specific features of VC formation in an annular REB by using the results of 3D fully electromagnetic simulations. First of all, we will analyze how the conditions for VC formation in an annular REB vary as the magnitude of the external magnetic field B_0 increases from 0 to 40 kG. The critical current was defined as the current value above which a reflected current produced by the beam electrons reflected from the VC appeared in the system. Here, by reflected electrons we mean electrons the longitudinal velocity of which in a certain plane in the drift space corresponding to the region of VC formation changes its sign for the first time. In this case, the values of the transmitted and reflected currents fluctuate in time with a frequency proportional to the plasma frequency ω_p of the REB, i.e., an unsteady VC forms, the oscillation frequency of which is determined by the REB plasma frequency [1, 3, 14]. This leads to the excitation of microwave electromagnetic waves at the VC oscillation frequency, from which we also detected the formation of an oscillating VC in the beam. This allowed us to determine the instant of VC formation and, accordingly, the REB critical current with a high accuracy.

Figure 1a shows the REB critical current I_{cr} at which an unsteady VC forms in the system as a function of the external magnetic field B_0 for different values of the energy W_e of the injected beam electrons. These dependences reflect the conditions for VC formation in an annular REB in a finite uniform external magnetic field. For comparison, the inset in Fig. 1a shows the corresponding values of the critical current for a weakly relativistic annular beam, taken from [40, 43].

It can be seen from Fig. 1a that, in the range of external magnetic fields from 0 to B^i_{max}, there is a region in which the REB critical current increases with increasing external magnetic field (a typical dependence of the REB critical current on the magnitude of the external magnetic field with characteristic values of this field is shown in Fig. 1b). For ultrarelativistic beams with electron energies of $W_e > 0.6$ MeV (Fig. 1a; curves *3*, *4*), the critical current begins to increase immediately at $B_0 > 0$. At lower energies of injected electrons, the increase in the critical current takes place for external magnetic fields of $B_0 \geq B^i_{ch}$ (Fig. 1a; curves *1*, *2*). If the electron beam is weakly relativistic (or nonrelativistic), such an increase in the critical current is not observed at all (see the inset in Fig. 1a) and the dependence $I_{cr}(B_0)$ is monotonically descending.

For greater magnitudes of the external magnetic field, $B_0 > B^i_{max}$, the critical current decreases monotonically with increasing B_0 at any energy of injected electrons (Fig. 1a), and, at $B_0 \sim B^i_{min}$, it saturates at a relatively low constant level.

Let us compare the REB critical current in a strong magnetic field ($B_0 = 40$ kG), at which the dynamics of the beam electrons can be considered practically one-dimensional, with the limiting vacuum current defined by formula (1). Figure 2 shows the REB critical current calculated at $B_0 = 40$ kG for different values of the energy W_e of injected electrons (symbols) and the current I_{SCL} calculated by analytic formula (1) for a fully magnetized REB. It is seen that these dependences are in good quantitative and qualitative agreement, which indicates that the analytic and numerical models correctly describe the REB behavior in 3D geometry.

Thus, analysis of the behavior of the critical current at which an unsteady oscillating VC forms in the REB shows that a local minimum in the dependence of the critical current on the external magnetic field appear at a certain value of the magnetic field, $B_0 = B^i_{max}$ (see Fig. 1a). Such behavior is not observed at small electron energies and takes place as the beam current increases and electron energies become relativistic.

3.2. Physical Processes Resulting in VC Formation in an REB at Low External Magnetic Fields

Analysis of the physical processes occurring in an REB shows that the character of the dependences $I_{cr}(B_0)$ presented in Fig. 1a is determined by the influence of the REB magnetic self-field on the beam dynamics and, accordingly, on the conditions of VC formation. As a result, this effect is most clearly pronounced at small values of the external magnetic field and high energies of injected electrons, $W_e > 0.6$ MeV.

Let us consider this issue in more detail. Figures 3–5 present typical configuration portraits of an REB—projections of the instantaneous positions (z_i, r_i, θ_i) of model particles simulating the REB onto the longitudinal (z, r) and transverse (r, θ) cross sections of the interaction space—at beam currents close to the critical one ($I \geqslant I_{cr}(B_0)$) and different characteristic values of the external magnetic field B_0. Figure 3 corresponds to the magnetic field value lying to the left from the maximum of curve *1* in Fig. 1 ($B_0 < B^1_{max}$), Fig. 4 corresponds to the magnetic field lying near the local maximum ($B_0 \sim B^1_{max}$), and Fig. 5 corresponds to the

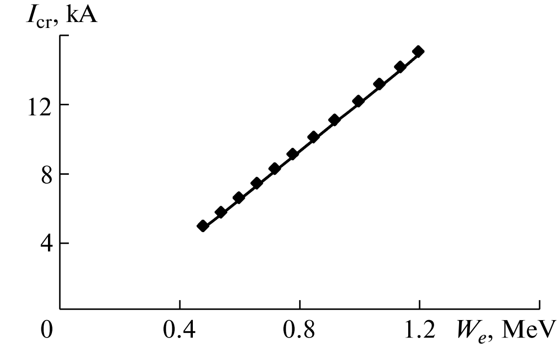

Fig. 2. Comparison of the REB critical currents calculated by analytic formula (1) (solid line) and calculated numerically (symbols) for the magnetic field $B_0 = 40$ kG, at which the beam dynamics is close to one-dimensional, and different values of the initial electron energy W_e.

region where the dependence $I_{cr}(B)$ saturates at a constant level ($B_0 \geqslant B^1_{min}$). All these portraits were obtained for an electron energy of $W_e = 0.48$ MeV.

It turns out that, at sufficiently low external magnetic fields, $0 \leq B_0 \leq B^i_{max}$ (see Fig. 1b), the electron dynamics in an REB near the minimum of the potential (in the VC region) differs radically from that in the case of a weakly relativistic or nonrelativistic beam. It is found that, in this case, the electron beam is unstable in a wide range of REB currents, which leads to both strong radial inhomogeneity of the electron beam and loss of its azimuthal symmetry.

The instability of an initially axisymmetric beam is caused by the strong magnetic self-field of the REB. Indeed, the vector of the azimuthal magnetic self-field B^s_θ generated by the longitudinal beam current (i.e., the current produced by charged particles having the longitudinal velocity component v_z) lies in the transverse cross section of the interaction space [56]. At the same time, since there is a significant transverse current produced by electrons having the radial velocity component v_r due to the incomplete suppression of the beam radial divergence by the external magnetic field, the longitudinal component B^s_z of the magnetic self-field appears. This leads to an increase in the azimuthal Lorentz force acting on the beam electrons moving in the transverse direction. As a result, they acquire an azimuthal velocity; i.e., due to its magnetic self-field, the REB begins to rotate as a whole about it symmetry axis. In this case, due to the action of the centrifugal force on the rotating electrons, a vortex structure forms in the beam, which leads to strong azimuthal asymmetry of the beam and perturbation of the beam boundary. Due to the onset of the beam instability, the current escaping onto the wall of the interaction space near the injection plane increases substantially.

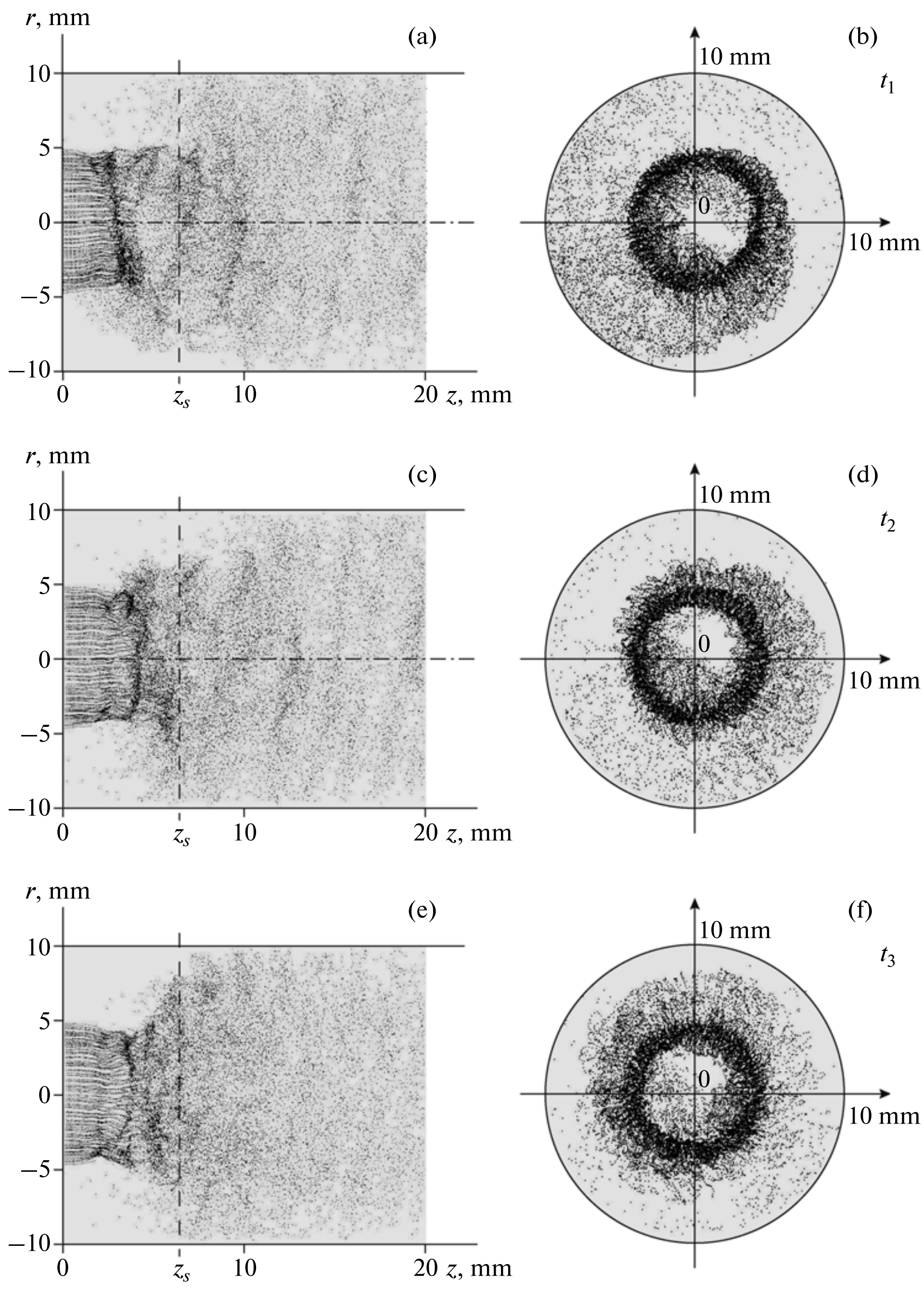

Fig. 3. Projections of the instantaneous positions of model particles of an electron beam onto the planes (z, r) (on the left) and (r, θ) (on the right) at $z = 6$ mm and successive instants of time with steps of $\Delta t = 0.1$ ns between the first and second frames and $\Delta t = 0.2$ ns between the second and third frames for $B = 3$ kG, $I = 7.5$ kA, and $W_e = 0.48$ MeV. The particles situated behind the projection plane are shown in the configuration portraits. The vertical dashed lines in Figs. 3a, 3c, and 3e denote the plane onto which the positions of model particles in Figs. 3b, 3d, and 3f are projected.

The rotation of the resulting vortex structure in the drift space can be traced by comparing the configuration portraits of the beam in Figs. 3b, 3d, and 3f, corresponding to different instants t_i. The cross section of the interaction space in these figures corresponds to $z_s = 6$ mm. It should be noted that the physical mechanism of the observed instability has much in common with the well-known convective instability of a beam that develops in a finite longitudinal external magnetic field due to the radial inhomogeneity of the density and velocity of the beam electrons [5, 57, 58]. In our case, however, such an inhomogeneity arises due to the

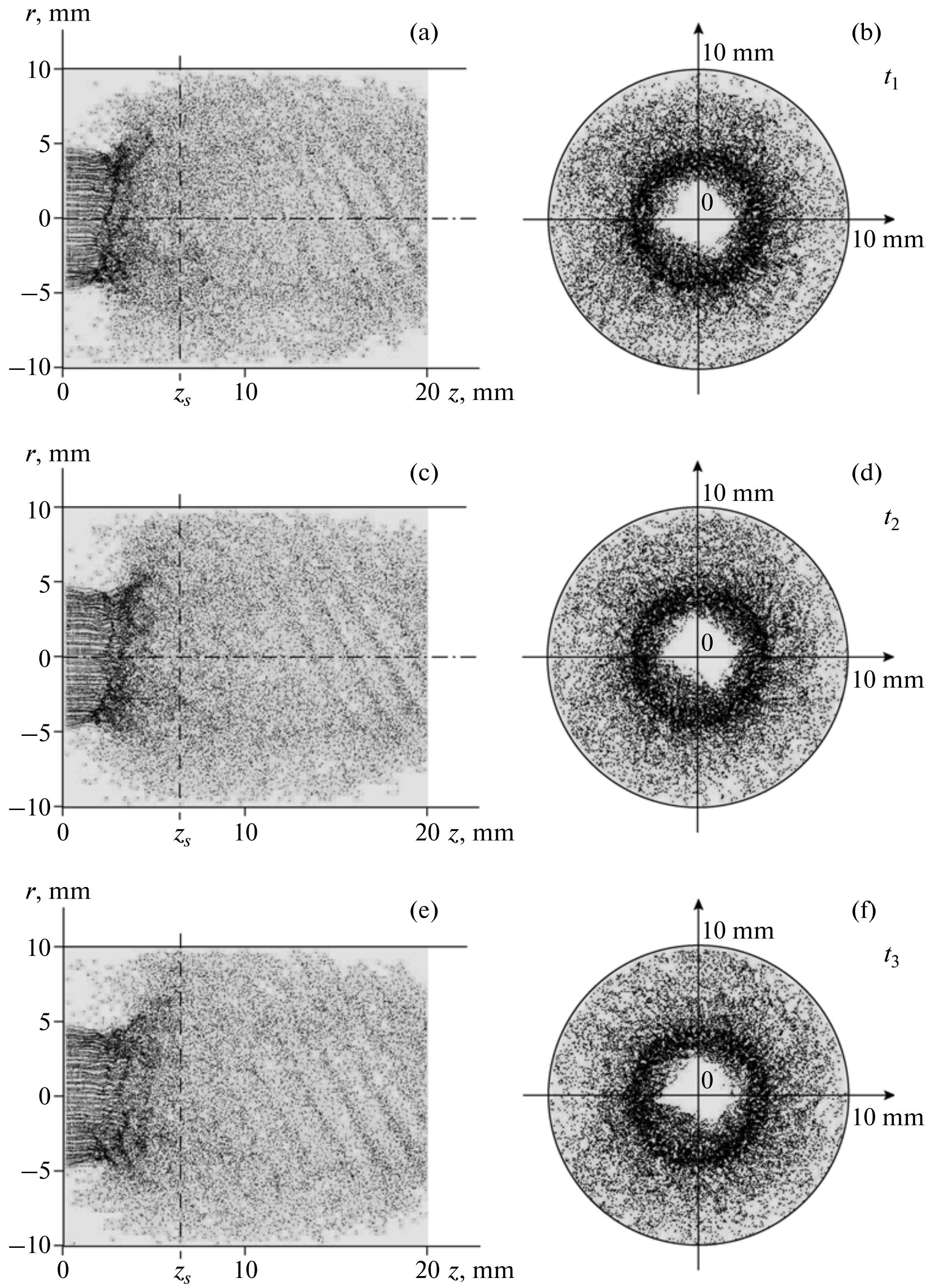

Fig. 4. Projections of the instantaneous positions of model particles of an electron beam onto the planes (z, r) (on the left) and (r, θ) (on the right) at $z = 6$ mm and successive instants of time with a step of $\Delta t = 0.2$ ns between the frames for $B = 5$ kG, $I =$ 9 kA, and $W_e = 0.48$ MeV. The particles situated behind the projection plane are shown in the configuration portraits. The vertical dashed lines in Figs. 4a, 4c, and 4e denote the plane onto which the positions of model particles in Figs. 4b, 4d, and 4f are projected.

interaction of the REB with its self-field, rather than with the external field.

The revealed instability of the REB leads to a reduction in the critical beam current required for VC formation due to a decrease in the longitudinal electron energy and an increase in the velocity scatter in the interaction space. As a result, due to the large number of electrons with low velocities, a VC forms in the region where the vortex structure forms and where the REB space charge is maximum. Figures 3a, 3c, and 3e demonstrate a typical picture of the VC forma-

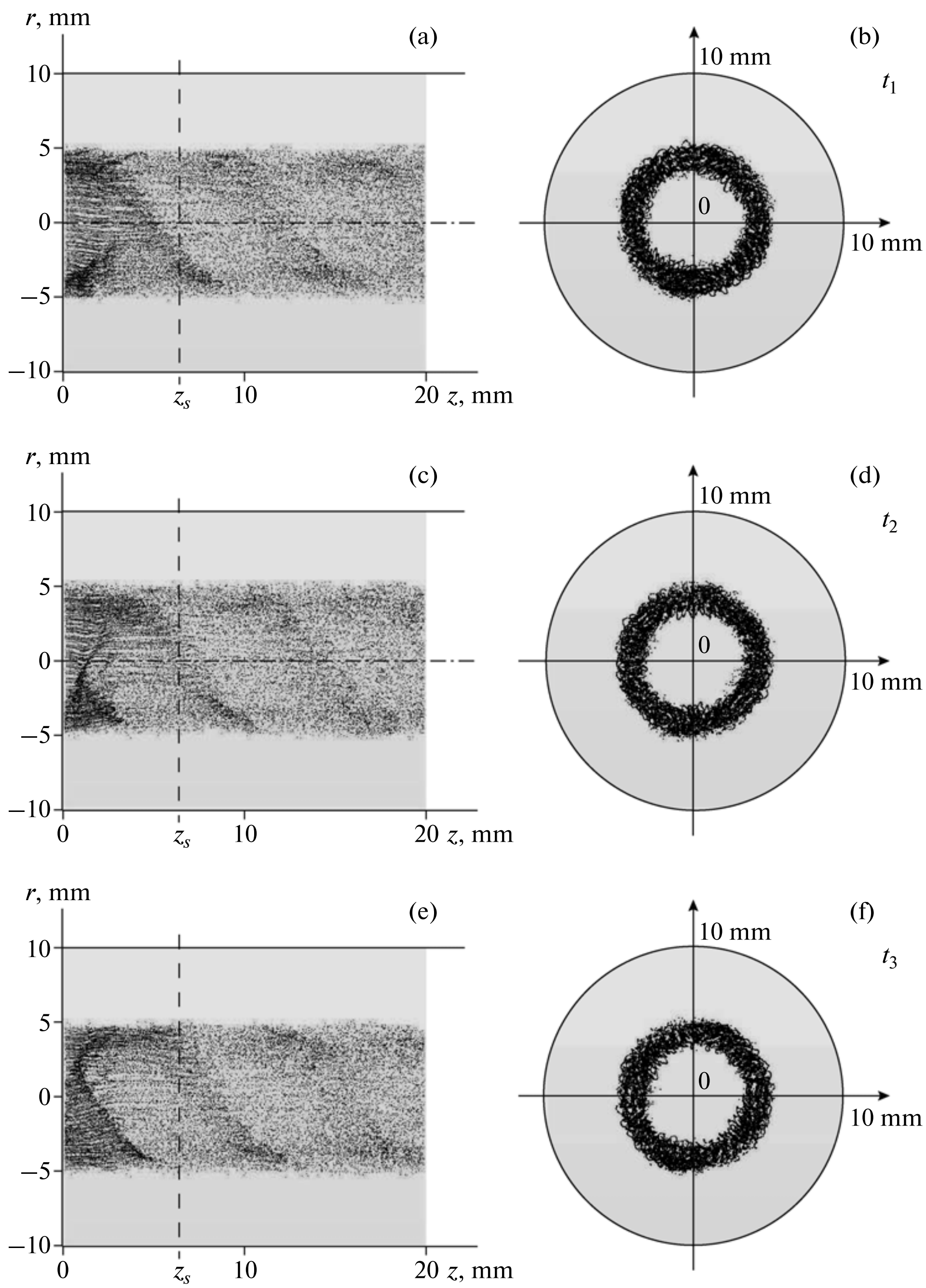

Fig. 5. Projections of the instantaneous positions of model particles of an electron beam onto the planes (z, r) (on the left) and (r, θ) (on the right) at $z = 6$ mm and successive instants of time with a step of $\Delta t = 0.2$ ns between the frames for $B = 30$ kG, $I =$ 10 kA, and $W_e = 0.48$ MeV. The particles situated behind the projection plane are shown in the configuration portraits. The vertical dashed lines in Figs. 5a, 5c, and 5e denote the plane onto which the positions of model particles in Figs. 5b, 5d, and 5f are projected.

tion and REB dynamics in the plane (z, r) ($\theta = 0$) in this case. It can be seen that a VC (due to the higher charge density, it manifests itself as the dark region in the configuration portraits) forms near the injection plane. It is spatially asymmetric and makes small-amplitude longitudinal oscillations about its average position (cf. Figs. 3a, 3c, 3e).

As the external magnetic field increases, azimuthal instability is suppressed, because the focusing force of the external magnetic field is directed oppositely to the centrifugal force acting on rotating electrons. At electron energies on the order of $W_e \approx 0.4$–0.7 MeV, an increase in the critical current takes place in the range of external magnetic fields from $B^i_{\rm ch}$ to $B^i_{\max}$ (see Fig. 1a; curves *1*, *2*). At higher energies of the beam electrons, such an increase takes place in the range from 0 to $B^i_{\max}$ (Fig.1a; curves *3*, *4*). This effect is illustrated by Fig. 4, which is plotted for an external magnetic field of $B_0 \sim B^1_{\max}$, which corresponds to the local maximum in the dependence $I_{\rm cr}(B_0)$ (see Fig. 1a). Indeed, as is seen from Figs. 4b, 4d, and 4f, the vortex electron structure rotating in the azimuthal direction is suppressed and the electrons fill the interaction space without substantial azimuthal inhomogeneities. In this regime, the space charge density decreases and the critical current required for VC formation increases. As is with the case of a lower magnetic field, the REB rotates as a whole in the azimuthal direction and the VC (observed as a dense bunch in Figs. 4a, 4c, and 4e) executes oscillations about its average position. It is worth noting that, in this case, the beam electrons still continue to drift toward the side wall of the interaction space, but this drift is restricted by the increased force of the external focusing magnetic field.

As the external magnetic field increases further ($B_0 \ge B^i_{\max}$), the critical REB current decreases monotonically and then (at $B_0 \sim B^i_{\min}$) saturates at a constant level. Such behavior at $B_0 \ge B^i_{\max}$ is caused by the suppression of the transverse dynamics of the beam electrons by the focusing external magnetic field. As a result, the critical current decreases due to an increase in the space charge density in the REB. The value of $B^i_{\min}$ corresponds to the external magnetic field at which the REB transverse dynamics is suppressed completely. This mechanism is similar to the mechanism revealed early in [40, 43] for a weakly relativistic beam (see also the inset in Fig. 1a). It follows from Fig. 5 that, in a strong external magnetic field ($B_0 \ge B^i_{\min}$), the transverse dynamics of charged particles is absent and no widening of the beam in the radial direction takes place.

The value of $B^i_{\min}$ can be found taking into account that the external magnetic field in this mode is already sufficiently strong and the magnetic self-field of the REB can be ignored. Let a beam with the critical current $I_{\rm cr}$ and initial radius R_b have a typical radius $R_{\rm VC}$ in the VC region. Due to the action of the REB electric self-field, we have $R_{\rm VC} > R_b$. It is known [46] that the angular momentum acquired by the beam electrons as they propagate in a uniform external magnetic field between points with the radii R_b and $R_{\rm VC}$ is proportional to the difference of the magnetic fluxes through the corresponding cross sections of the surface formed by the revolution of electrons about the beam axis,

$$R^2_{\rm VC}\frac{d\theta}{dt} = \frac{\pi\eta B_0}{2\pi\gamma_0}\left(R^2_{\rm VC} - R^2_b\right), \tag{5}$$

where $d\theta/dt$ is the azimuthal electron velocity, η is the electron charge-to-mass ratio, and γ_0 is the relativistic factor of the injected beam. Taking into account relationship (5) and that the radial motion of the beam electrons is determined by the centrifugal force $F_c = \gamma_0 m_e r(d\theta/dt)^2$, the Coulomb repulsion force $F_k = -eE_r$, and the Lorentz force $F_{\rm L} = -er(d\theta/dt)B_0$ (where e and m_e are the electron charge and mass, respectively; r is the radial coordinate of an electron; and E_r is the radial component of the REB electric self-field), we can write the dynamic equation for the beam boundary,

$$\frac{d^2r}{dz^2} + \frac{\eta B_0^2}{8V_0\gamma_0}R_{\rm VC}\left[1-\left(\frac{R_b}{R_{\rm VC}}\right)^4\right] - \frac{I\sqrt{\gamma_0}}{4\pi\varepsilon_0\sqrt{2\eta}V_0^{3/2}R_{\rm VC}} = 0, \tag{6}$$

where V_0 is the accelerating voltage and it is taken into account that $d^2r/dt^2 = (2\eta V_0/\gamma_0)d^2r/dz^2$.

This equation implies that there is a value of the external magnetic field $B^i_{\min}$ at which the beam radius is conserved. Indeed, if we set $d^2r/dz^2 = 0$ in Eq. (6), which means that the beam does not expand in the radial direction, then we obtain a quadratic equation with respect to B_0, the solution of which yields the value of the external magnetic field $B^i_{\min}$ at which the dependence $I_{\rm cr}(B_0)$ saturates (see Fig. 1),

$$B^i_{\min} = R_{\rm VC}\sqrt{\frac{\sqrt{2}I\gamma_0^{3/2}}{\pi\varepsilon_0\eta^{3/2}\sqrt{V_0}(R^4_{\rm VC} - R^4_b)}}. \tag{7}$$

Figure 6 shows analytic dependence (7) and the calculated values of $B^i_{\min}$ for an annular REB versus the energy W_e of injected electrons. It can be seen that dependence (7) agrees well with the simulations results. The value of $B^i_{\min}$ increases with increasing beam energy. This is caused by an increase in the electron inertia (the relativistic increase in the electron mass) with increasing initial energy W_e of the beam electrons. Therefore, the focusing of the beam electrons by the external magnetic field (i.e., the suppression the REB transverse dynamics) requires greater values of the external magnetic field, due to which $B_{\min}$ increases monotonically. It also follows from Fig. 6 that the behavior of the dependence $B_{\min}(W_e)$ is qualitatively the same for both weakly relativistic and relativistic values of W_e.

3.3. Physical Processes Occurring at Different REB Energies

Comparison of curves *1* and *2* with curves *3* and *4* in Fig. 1a shows that there is a characteristic value of the electron energy W^c_e above which the behavior of

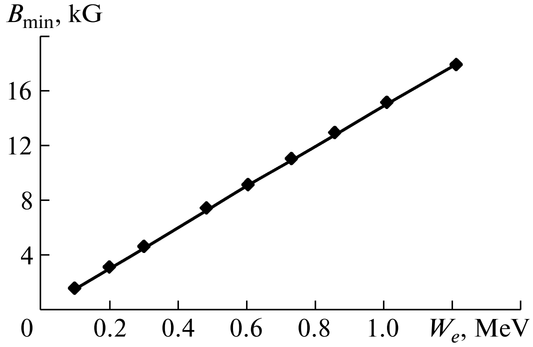

Fig. 6. Comparison of the values of the external magnetic field $B^i_{\min}$ determined by formula (1) (solid line) and calculated by means of 3D numerical simulations (symbols) for an annular REB vs. initial electron energy W_e.

the dependence $I_{\rm cr}(B_0)$ within the interval $(0, B^i_{\max})$ changes qualitatively, namely, the range of B_0 values in which the critical current decreases with increasing magnetic field disappears. Let us consider the physical processes resulting in such a change in the system behavior.

As the external magnetic field in the interval $(0, B^i_{\max})$ increases, the azimuthal instability of the beam is suppressed, which leads to an increase in the critical current. On the other hand, the transverse dynamics of charged particles is also suppressed, which leads to a decrease in the critical current. The growth rate of azimuthal instability increases with increasing initial electron energy W_e, because the Lorentz force responsible for this instability increases in proportion to the squared velocity of the injected beam: $F_{\rm L} \sim v_0 B^s \sim v_0 I_0 \sim v_0^2 \sim W_e$, where $F_{\rm L}$ is the Lorentz force and B^s is the REB magnetic self-field. Therefore, an increase in the initial electron energy accelerates azimuthal instability and favors the formation of a vortex structure. It follows from the aforesaid that, at relatively small electron energies, $W_e < W_e^c$, when the influence of azimuthal instability can be ignored, an increase in the external magnetic field leads to a reduction in the critical current due to the suppression of the transverse dynamics of charged particles in the beam; then, the critical current increases again due to the strong suppression of azimuthal instability (Fig. 1a; curves *1*, *2*). As the initial electron energy increases, the influence of azimuthal instability at low external magnetic fields also increases and begins to play the governing role in the process of VC formation. Therefore, suppression of azimuthal instability leads to a substantial increase in the REB critical beam. As a result, the height of the maximum in the dependence $I_{\rm cr}(B_0)$ (see Fig. 1a) increases with increasing initial electron energy W_e. This is clearly seen from comparison of curves *1*–*4* in Fig. 1a, which correspond to progressively increasing values of W_e in the range of relatively low magnetic fields.

At higher initial electron energies, $W_e > W_e^c$ (Fig. 1a; curves *3*, *4*), an increase in the external magnetic field in the range $(0, B^i_{\max})$ immediately leads to an increase in the critical current, because, in this case, azimuthal instability is the main mechanism resulting in VC formation. Even a partial suppression of this instability by the external magnetic field leads to an increase in the critical current. As a result, the critical current increases monotonically with increasing magnetic field in the range $(0, B^i_{\max})$.

Thus, W_e^c is the characteristic value of the initial electron energy above which the relationship between the physical processes occurring in the course of VC formation in an REB at low external magnetic fields changes. To illustrate this, let us consider the dependence of the critical current as a function of the electron energy in the absence of an external magnetic field, $B_0 = 0$ (see Fig. 7). We can see that this dependence has three characteristic sections. The first section corresponds to REB energies in the range of 0–0.6 MeV and exhibits a monotonic increase in the REB critical current due to an increase in the depth of the potential well required for electron deceleration and VC formation. Such an increase in the depth of the potential well is achieved due to an increase in the space charge density of the beam at a fixed initial electron energy. In the second section of the dependence $I_{\rm cr}(W_e)$, which corresponds to $W_e \in 0.6$–1.0 MeV, the REB critical current decreases monotonically with increasing W_e. This is caused by an increase in the influence of azimuthal instability of the REB with increasing W_e. The growth rate of this instability is proportional to the electron energy. The decrease in the REB critical current caused by azimuthal instability at large values of W_e and low values of the external magnetic field prevails over the increase in $I_{\rm cr}$ caused by an increase in the depth of the potential well; as a result, the REB critical current decreases with increasing W_e. In the third section of the dependence of the critical REB current on W_e at $B_0 = 0$ ($W_e > 1$ MeV), $I_{\rm cr}$ again increases monotonically with increasing W_e. Such behavior of the critical current at high REB energies is caused by the strong influence of relativistic effects (see Section 3.2). Indeed, at high initial electron energies, the process of VC formation in the REB is significantly affected by the relativistic increase in the electron mass. In this case, the formation of an unsteady VC requires a higher space charge density, due to which the REB critical current increases with increasing initial electron energy W_e.

Thus, the dependence of the REB critical current on the initial electron energy at low external magnetic fields exhibits a rather complicated behavior. This is

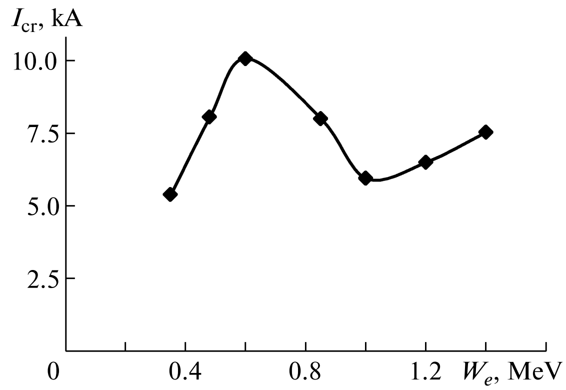

Fig. 7. Critical current of an annular REB vs. initial electron energy W_e in the absence of an external magnetic field.

caused by the competition of different factors, such as an increase in the critical current with increasing initial electron energy, azimuthal instability of the REB, and the relativistic increase in the electron mass.

4. CONCLUSIONS

Summarizing the results obtained in this study, we can conclude that the conditions and mechanisms of VC formation in relativistic and ultrarelativistic electron beams have specific features making them different from those in a weakly relativistic case. With the help of 3D electromagnetic simulations, it is found how the REB critical current at which an unsteady oscillating VC forms in the system depends on the system parameters (such as the magnitude of the external magnetic field and the beam electron energy). It is shown that, in the absence of an external focusing magnetic field, the conditions for VC formation are determined by the influence of the REB magnetic self-field. Azimuthal instability of the electron beam caused by the action of the REB magnetic self-field, which leads to a decrease in the REB critical current, has been revealed. This instability results in a reduction in the critical current at low external magnetic fields and high energies of injected electrons. An increase in the external longitudinal magnetic field leads to the suppression of this type of azimuthal instability of the REB in the magnetic self-field and an increase in the critical current. At strong external magnetic fields, the critical current decreases and then saturates, as is the case with a nonrelativistic electron beam [43]. The magnetic field at which the critical current saturates is determined by analytic formula (7). In this case, the current at which a VC forms in the system agrees well with formula (1), obtained in the 1D model.

ACKNOWLEDGMENTS

We are grateful to Prof. I.I. Magda for fruitful discussions of the results obtained. This work was supported by the Ministry of Education and Science of the Russian Federation (contract no. 14.B37.21.0764), the Russian Foundation for Basic Research (project nos. 12-02-00345-a and 12-02-31102), and the Russian Federation Presidential Program (project nos. MD-345.2013.2 and MK-818.2013.2).

REFERENCES

1. *High-Power Microwave Sources (Artech House Microwave Library)*, Ed. by V. L. Granatstein and I. Alexeff (Artech House, Boston,1987).
2. A. E. Dubinov and V. D. Selemir, J. Comm. Technol. Electron. **6**, 575 (2002).
3. D. I. Trubetskov and A. E. Khramov, *Lectures on Microwave Electronics for Physicists* (Fizmatlit, Moscow, 2003, 2004), Vols. 1, 2 [in Russian].
4. L. S. Bogdankevich and A. A. Rukhadze, Sov. Phys. Usp. **14**, 163 (1971).
5. M. V. Kuzelev, A. A. Rukhadze, and P. S. Strelkov, *Plasma Relativistic Microwave Electronics* (Mosk. Gos. Tekhn. Univ. im. N.E. Baumana, Moscow, 2002) [in Russian].
6. C. K. Birdsall and W. B. Bridges, *Electron Dynamics of Diode Regions* (Academic, New York, 1966).
7. R. A. Mahaffey, P. A. Sprangle, J. Golden, and C. A. Kapetanakos, Phys. Rev. Lett. **39**, 843 (1977).
8. A. N. Didenko, Ya. E. Krasik, S. F. Perelygin, and G. P. Fomenko, Sov. Tech. Phys. Lett. **5**, 128 (1979).
9. V. G. Anfinogentov and A. E. Khramov, Radiophys. Quant. Electron. **41**, 764 (1998).
10. W. Jiang, K. Masugata, and K. Yatsui, Phys. Plasmas **2**, 982 (1995).
11. A. A. Koronovskii and A. E. Khramov, Plasma Phys. Rep. **28**, 666 (2002).
12. D. Biswas, Phys. Plasmas **16**, 063104 (2009).
13. H. Sze, J. Benford, and T. Young, IEEE Trans. Plasma Sci. **15**, 592 (1985).
14. A. N. Didenko and V. I. Rashchikov, Sov. J. Plasma Phys. **18**, 616 (1992).
15. V. D. Selemir, B. V. Alekhin, V. E. Vatrunin, et al., Plasma Phys. Rep. **20**, 621 (1994).
16. Yu. A. Kalinin, A. A. Koronovskii, A. E. Khramov, et al., Plasma Phys. Rep. **31**, 938 (2005).
17. E. N. Egorov, Yu. A. Kalinin, Yu. I. Levin, et al., Izv. Ross. Akad. Nauk, Ser. Fiz. **69**, 1724 (2005).
18. E. N. Egorov and A. E. Hramov, Plasma Phys. Rep. **32**, 683 (2006).
19. G. Singh and Ch. Shashank, Phys. Plasmas **18**, 063104 (2011).
20. A. E. Khramov, J. Comm. Technol. Electron. **44**, 551 (1999).
21. E. N. Egorov, Yu. A. Kalinin, A. A. Koronovskii, et al., J. Comm. Technol. Electron. **52**, 45 (2007).
22. A. E. Dubinov and I. A. Efimova, Tech. Phys. **48**, 1205 (2003).

23. R. A. Filatov, A. E. Hramov, Y. P. Bliokh, et al., Phys. Plasmas **16**, 033106 (2009).
24. A. A. Rukhadze, A. S. Bogdankevich, S. E. Rosinskii, and V. G. Rukhlin, *Physics of High-Current Relativistic Electron Beams* (Atomizdat, Moscow, 1980) [in Russian].
25. M. V. Kuzelev and A. A. Rukhadze, *Electrodynamics of Dense Electron Beams in Plasma* (Nauka, Moscow, 1990) [in Russian].
26. A. V. Fedotov and A. G. Shkvarunets, Sov. J. Plasma Phys. **14**, 405 (1988).
27. V. I. Krementsov, P. S. Strelkov, and A. G. Shkvarunets, Sov. J. Plasma Phys. **2**, 519 (1976).
28. P. A. Lindsay, W. K. Toh, and X. Chen, IEEE Trans. Plasma Sci. **30**, 1186 (2002).
29. X. Chen, W. K. Toh, and P. A. Lindsay, IEEE Trans. Plasma Sci. **32**, 835 (2004).
30. A. E. Dubinov, I. A. Efimova, I. Yu. Kornilova, et al., Fiz. Element. Chast. At. Yadra **35**, 462 (2004).
31. E. N. Egorov, S. A. Kurkin, and A. E. Khramov, *Influence of Two-Dimensional Effects of Charge Particle Dynamics on Oscillations in Electron Flows with a Virtual Cathode. Methods of Nonlinear Dynamics and Chaos Theory in Problems of Microwave Electronics* (Fizmatlit, Moscow, 2009), Vol. 2: *Nonstationary and Chaotic Processes* [in Russian].
32. A. E. Khramov, S. A. Kurkin, E. N. Egorov, et al., Mat. Model. **23** (1), 3 (2011).
33. J. Wang, Z. Chen, Y. Wang, et al., Phys. Plasmas **17**, 073107 (2010).
34. R. A. Filatov and A. E. Hramov, Plasma Phys. Rep. **37**, 395 (2011).
35. H. Sze, J. Benford, and B. Harteneck, Phys. Fluids **29**, 5875 (1986).
36. A. E. Dubinov and V. D. Selemir, Tech. Phys. Lett. **27**, 557 (2001).
37. A. E. Hramov, A. A. Koronovskii, and S. A. Kurkin, Phys. Lett. A **374**, 3057 (2010).
38. S. A. Kurkin, A. A. Koronovskii, and A. E. Hramov, Tech. Phys. Lett. **37**, 356 (2011).
39. J. Benford, J. A. Swegle, and E. Schamiloglu, *High-Power Microwaves* (CRC Press, Boca Raton, 2007).
40. S. A. Kurkin, A. A. Koronovskii, and A. E. Hramov, Tech. Phys. **54**, 1520 (2009).
41. M. Yu. Morozov and A. E. Hramov, Plasma Phys. Rep. **33**, 553 (2007).
42. A. E. Hramov, A. A. Koronovskii, M. Yu. Morozov, and A. V. Mushtakov, Phys. Lett. A **372**, 876 (2008).
43. S. A. Kurkin, A. A. Koronovskii, and A. E. Hramov, Plasma Phys. Rep. **35**, 628 (2009).
44. V. A. Balakirev, A. M. Gorban', I. I. Magda, et al., Plasma Phys. Rep **23**, 323 (1997).
45. A. E. Dubinov, I. Yu. Kornilova, and V. D. Selemir, Phys. Usp. **45**, 1109 (2002).
46. S. E. Tsimring, *Electron Beams and Microwave Vacuum Electronics* (Wiley, Hoboken, NJ, 2007).
47. G. A. Mesyats, *Pulsed Energetics and Electronics* (Nauka, Moscow, 2004) [in Russian].
48. I. L. Bogdankevich, P. S. Strelkov, V. P. Tarakanov, and D. K. Ul'yanov, Plasma Phys. Rep. **30**, 376 (2004).
49. A. S. Roshal', *Modeling of Charged Beams* (Atomizdat, Moscow, 1979) [in Russian].
50. Ch. K. Birdsall and A. B. Langdon, *Plasma Physics via Computer Simulation* (McGraw-Hill, New York, 1985).
51. A. G. Sveshnikov and S. A. Yakunin, Mat. Model. **1** (4), 1 (1989).
52. T. M. Anderson, A. A. Mondelli, B. Levush, et al., Proc. IEEE **87**, 804 (1999).
53. A. D. Grigor'ev, Izv. Vyssh. Uchebn. Zaved., Prikl. Nelin. Dinam. **7** (4), 48 (1999).
54. V. G. Anfinogentov and A. E. Khramov, J. Comm. Technol. Electron. **5**, 546 (2001).
55. J. P. Boris and R. Lee, Comm. Math. Phys. **12**, 131 (1969).
56. R. C. Davidson, *Theory of Nonneutral Plasmas* (Benjamin, New York, 1974).
57. R. H. Levy, Phys. Fluids **8**, 1288 (1965).
58. A. L. Peratt and C. M. Snell, Phys. Rev. Lett. **54**, 1167 (1985).

Translated by E. Chernokozhin